Geophysical Journal International

Geophys. J. Int. (2012) **190,** 856–870 doi: 10.1111/j.1365-246X.2012.05542.x

Magnetic energy transfer at the top of the Earth's core

Ludovic Huguet* and Hagay Amit

CNRS UMR 6112, Université de Nantes, Laboratoire de Planétologie et de Géodynamique, 2 rue de la Houssinière, Nantes, F-44000, France.
E-mail: Hagay.Amit@univ-nantes.fr

Accepted 2012 May 8. Received 2012 May 7; in original form 2011 July 15

SUMMARY

We introduce a formalism to track magnetic energy transfer between spherical harmonic degrees due to the interaction of fluid flow and radial magnetic field at the top of the Earth's core. Large-scale synthetic single harmonic flows are characterized by a fixed difference between harmonics participating in the transfer. Large-scale toroidal flows result in more local energy transfer than small-scale poloidal flows. Axisymmetric poloidal flows are most efficient in producing energy transfer and dipole changes. The azimuthal phase relation between the field and the flow may play a major role in the energy transfer. Geomagnetic energy transfer induced by core flow models exhibit a striking transfer spectrum pattern of alternating extrema suggestive of energy cascade, but the detailed transfer spectrum matrix reveals rich behaviour with both local Kolmogorov-like transfer and non-local transfer, the latter about twice larger. The transfer spectrum reverses from even maxima and odd minima between 1840 and 1910 to odd maxima and even minima between 1955 and 1990. The transfer spectrum matrix shows geomagnetic energy cascade from low to high degrees as well as non-local transfer from the dipole directly to higher degrees, explaining the simultaneous dipole decrease and non-dipole increase during the historical period.

Key words: Dynamo: theories and simulations; Geomagnetic induction; Magnetic field; Rapid time variations; Core, outer core and inner core.

1 INTRODUCTION

The geomagnetic field is generated by convection-driven flow of an electrically conducting fluid at the Earth's outer core. Measurements of the geomagnetic field and its secular variation (SV) may provide vital constraints on core dynamics. Geomagnetic field models based on surface observatories and recent satellite data (Jackson *et al.* 2000; Olsen & Mandea 2008) show that the radial field at the core–mantle boundary (CMB) is dominated by an axial dipole component. Since the advent of geomagnetic measurements about 170 yr ago, the geomagnetic dipole intensity has been rapidly decreasing (Olson & Amit 2006). The rate of dipole decrease has been varying significantly with time (Fig. 1).

Efforts to unravel the kinematic mechanisms responsible for the current dipole decrease focused mostly on a local-spatial approach. Gubbins (1987) used the integral form of the axial dipole $m_z \propto \int_S B_r \cos\theta dS$ (where B_r is the radial geomagnetic field on the CMB, θ is co-latitude and dS is a surface increment of the CMB) to identify CMB regions that provide positive/negative contributions to the axial dipole. He argued that the growth and intensification of reversed flux patches, especially below the southern Atlantic, are responsible for most of the dipole decrease. Emergence of reversed flux patches on the CMB and their deep core upwellings origin have been identified in many numerical dynamos as triggers to dipole collapse and subsequent polarity reversals (Wicht & Olson 2004; Takahashi *et al.* 2007; Aubert *et al.* 2008; Olson *et al.* 2009). Following Moffatt (1978), Olson & Amit (2006) derived an integral equation for mapping advective and diffusive contributions to axial dipole SV. They found that the combined effects of growth of reversed flux by magnetic diffusion, poleward advection of reversed flux and equatorward advection of normal flux by the flow, have worked in unison to decrease the dipole. Liu & Olson (2009) proposed a power law for the dipole decrease rate as a function of the magnetic Reynolds number.

Alternatively, dipole changes can be studied via a spectral approach. Degree–time plots obtained from numerical dynamo models show that during reversals the peak of poloidal magnetic field energy on the outer boundary moves progressively from the dipole to higher degrees, which is suggestive of a forward magnetic energy cascade (Olson *et al.* 2009; Amit & Olson 2010). Gissinger *et al.* (2010) argued that reversals in their low magnetic Prandtl number forced magnetohydrodynamic (MHD) simulations can be approximated by a simple set of differential equations representing energy exchange between the dipole and the quadrupole. Amit & Olson (2010) designed a spectral approach for studying dipole SV, and more generally, temporal variations in the Mauersberger–Lowes geomagnetic spectrum. They manipulated the radial magnetic induction equation to an equation for the SV of the Mauersberger–Lowes

*Now at: LGL, Laboratoire de Géologie de Lyon, CNRS, Université Lyon 1, ENS-Lyon, Géode, 2 rue Raphaël Dubois, 69622 Villeurbanne, France.

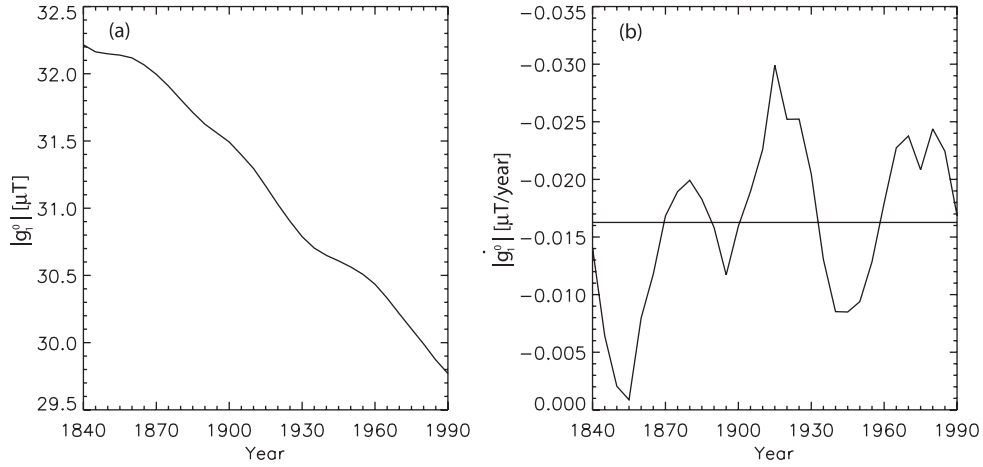

Figure 1. Absolute geomagnetic axial dipole Gauss coefficient $|g_1^0|$ in μT (a) and its SV $|\dot{g}_1^0|$ in $\mu\mathrm{T\,yr}^{-1}$ (b) based on the historical field model *gufm1* of Jackson *et al.* (2000) for the period 1840–1990. The horizontal line in (b) denotes the time-average axial dipole decrease rate.

spectrum. Motivated by classical turbulence theory, they assumed that magnetic energy is transferred locally between neighbouring spherical harmonic degrees. Their spectral transfer rates showed a persistent inverse energy cascade in the quadrupole family and a time-dependent forward energy cascade in the dipole family, consistent with the observed simultaneous dipole decrease and non-dipole increase during the historical era.

The local transfer assumption adopted by Amit & Olson (2010) is supported by non-magnetic and MHD turbulence theory and simulations. According to the classical turbulence theory of Kolmogorov, energy cascades between similar size eddies without major jumps between distinctive length scales (Kolmogorov 1941; Batchelor 1953; Frisch 1995). The energy at a certain degree is statistically decoupled from any large-scale energy source and is determined solely by the rate of energy transfer across the inertial range (Moffatt 1978). Numerical simulations of the time evolution of kinetic and magnetic energy and helicity (Pouquet *et al.* 1976) and helical kinematic dynamos (Mininni 2007) show that magnetic energy is progressively excited at larger scales as time increases, thus intensifying the large-scale field by inverse cascade of magnetic helicity. Numerical MHD simulations of turbulence find both local Kolmogorov-like and non-local transfers (Yousef *et al.* 2007; Mininni 2011). Forced MHD turbulence simulations show local magnetic energy transfer (Alexakis *et al.* 2005a; Carati *et al.* 2006). Local magnetic energy transfer was found to be associated with energy cascade by magnetic field advection, whereas non-local transfer was found to be associated with energy injected from the large scales directly into the small scales by magnetic field stretching induced by the poloidal flow (Alexakis *et al.* 2007). Amit & Olson (2010) argued that because the core flow is dominantly toroidal (see Finlay & Amit 2011, and references therein), local transfer is expected to dominate geomagnetic induction at the top of the core. Mininni (2011) summarized based on turbulence MHD simulations that the transfer of magnetic energy from one degree to another seems dominantly local, whereas non-local effects are more dominant in the transfer from kinetic to magnetic energy that generates the dynamo.

How important is the role of classical 3-D isotropic, homogeneous turbulence in the geodynamo? According to the very small estimates of the Rossby number in the Earth's core (Olsen & Mandea 2008), turbulence is expected to be negligible compared to rotational effects. However, estimates of the local Rossby number that rely on eddy size rather than system length scale suggest that turbulence in the Earth's core is nearly as important as rotation, and that inertial effects may play an important role in polarity reversals (Christensen & Aubert 2006; Olson & Christensen 2006). Alternatively, it is possible that boundary layer control rather than force balance determines the competition between turbulence and rotation. King *et al.* (2009) argued based on experiments and numerical simulations that the relation between the Ekman and thermal boundary layer thicknesses dictates whether the flow will be organized in equatorially symmetric columns or in random 3-D structures. According to their scaling laws, the Earth's core is not far from the transition between the rapidly rotating regime to the turbulent regime.

Direct evidence for turbulence in the core is difficult to obtain. The geomagnetic field reversals time-series can be fitted by a log-normal distribution that is suggestive of 'multiplicative noise' in the geodynamo due to a turbulent α-effect (Ryan & Sarson 2007). King *et al.* (2009) illustrated that deviations from equatorial symmetry may suggest the presence of turbulence in a rapidly rotating system. Some core flow models inferred from inversions of geomagnetic SV show persistent deviations from equatorial symmetry, most notably westward drift in mid-latitudes of the southern hemisphere without a northern counterpart (Jackson 1997; Pais & Hulot 2000; Amit & Olson 2006; Holme & Olsen 2006). Quasi-geostrophic core flow models which assume equatorial symmetry were found capable of explaining the SV (Pais & Jault 2008; Gillet *et al.* 2009, 2011). The core flow models of Schaeffer & Pais (2011) obtained without imposing equatorial symmetry contain 66–84 per cent (depending on the length scale) symmetric kinetic energy, that is, the flow is about half way between purely symmetric to equally symmetric/antisymmetric. Deviations from equatorial symmetry might also arise from the impact of the lower mantle heterogeneity on the geodynamo (Aubert *et al.* 2007; Gubbins *et al.* 2007), though possibly only on long timescales (Olson & Christensen 2002). The symmetry level of the flow in the Earth's core is still under debate.

In this paper, we introduce a formalism to track magnetic energy transfer between different spherical harmonic degrees in the Mauersberger–Lowes spectrum, which can be useful in identifying Kolmogorov-like turbulence signature at the top of the core. We forward solve the radial frozen-flux magnetic induction equation for a given flow and radial field models. The SV is transformed to Gauss coefficients, and in conjunction with the field Gauss

coefficients, the energy transfer between each pair of spherical harmonics within the observed spectrum is calculated. We apply our formalism to synthetic flows for intuitive physical understanding, and to core flow models inferred from the geomagnetic SV for geophysical interpretation. Our approach allows to test the local transfer assumption of Amit & Olson (2010) and to examine the possibility that the current geomagnetic dipole decrease is caused by a forward magnetic energy cascade. Furthermore, our method sheds light on the overall variability of the large-scale geomagnetic field spectrum during the historical period.

For given flow and field models, admissible magnetic energy transfers are constrained by the selection rules of the Gaunt and Elsasser integrals (Elsasser 1946). These rules dictate whether a certain flow is capable of converting toroidal magnetic field to poloidal and vice versa, and are therefore fundamental to kinematic dynamo theory (Bullard & Gellman 1954). Kahle *et al.* (1967) used the Gaunt and Elsasser integrals to invert for the flow at the top of the core from geomagnetic field and SV models. Whaler (1986) used the triangle rule to relate the maximum spherical harmonic degree of the flow with the sum of maximum degrees of the field and its SV. For our purposes, the selection rules are used to verify the validity of the energy transfers generated by synthetic flows.

Assessing energy transfer from the interaction between the core field and flow is obviously prone to errors due to uncertainties in these models. The historical field model *gufm1* of Jackson *et al.* (2000) might suffer from problems of insufficient data coverage and poor data quality. In general, geomagnetic field models constructed from observations are not constrained to obey the MHD equations and energy conservation is not implicit. Much more severe is the case of core flow models inferred from the geomagnetic SV, which are prone to numerous theoretical and practical sources of errors (Holme 2007). Any inference concerning the behaviour of the geomagnetic energy transfer during the historical period should therefore be taken with caution.

In addition, our analysis ignores the contribution of magnetic diffusion to the temporal changes of the geomagnetic energy spectrum. Magnetic diffusion SV is expected to be a localized phenomenon (Amit & Christensen 2008), so its impact on the large-scale spectrum is arguably secondary. Based on free decay formalisms using fundamental modes, magnetic diffusion was found to be generally negligible (Amit & Olson 2010). Nevertheless, the contribution of magnetic diffusion to the temporal changes of the geomagnetic spectrum is unknown.

The paper is outlined as follows. In Section 2 we describe our formalism, method, error estimates and graphical visualization of the results. Our energy transfer solutions for synthetic and core flow models are given in Section 3. We discuss our main findings in Section 4.

2 THEORY AND METHOD

The Mauersberger–Lowes spectrum at the CMB is one of the primary outputs of the dynamo process in the core (Dormy *et al.* 2000). The magnetic field spectrum R_n at the CMB can be expressed as a function of spherical harmonic degree n in terms of the Gauss coefficients of the core field as (Lowes 1974)

$$R_n = (n+1)\left(\frac{a}{c}\right)^{2n+4}\sum_{m=0}^{n}\left(\left(g_n^m\right)^2+\left(h_n^m\right)^2\right), \tag{1}$$

where a is the Earth's radius, c is the radius of the core and g_n^m and h_n^m are the Gauss coefficients of the core field at spherical harmonic degree and order n and m, respectively. The total magnetic energy is given by

$$\langle B_{\rm r}^2\rangle = \sum_{n}^{n_{\max}}\frac{n+1}{2n+1}R_n, \tag{2}$$

where $B_{\rm r}$ is the radial magnetic field on the CMB, $n_{\max}$ is the truncation level, and $\langle\rangle$ denotes CMB surface average. Similar to (1), the definition of the SV spectrum at the CMB is given by (Alldredge 1984; McLeod 1996; Voorhies 2004)

$$S_n = (n+1)\left(\frac{a}{c}\right)^{2n+4}\sum_{m=0}^{n}\left(\left(\dot{g}_n^m\right)^2+\left(\dot{h}_n^m\right)^2\right), \tag{3}$$

where the dots denote time derivatives. Using (1), the temporal variation of the field spectrum is written as (Cain *et al.* 1989)

$$\dot{R}_n = 2(n+1)\left(\frac{a}{c}\right)^{2n+4}\sum_{m=0}^{n}\left(g_n^m\dot{g}_n^m+h_n^m\dot{h}_n^m\right). \tag{4}$$

From (2), the temporal variation of the total magnetic energy is

$$\frac{\partial}{\partial t}\langle B_{\rm r}^2\rangle = \sum_{n}^{n_{\max}}\frac{n+1}{2n+1}\dot{R}_n. \tag{5}$$

Note that $\dot{R}_n$ has units of $\mu\mathrm{T}^2\,\mathrm{yr}^{-1}$, whereas S_n has units of $\mu\mathrm{T}^2\,\mathrm{yr}^{-2}$. Moreover, S_n is positive by definition, whereas $\dot{R}_n$ may acquire both signs. While R_n and S_n define the energy at each spherical harmonic degree of the field and SV, respectively, $\dot{R}_n$ is the rate of change of the energy at each degree.

Fig. 2 shows the three spectra for three arbitrary snapshots from the geomagnetic field and SV model *gufm1* of Jackson *et al.* (2000). From hereafter, we shall consider the field model up to degree

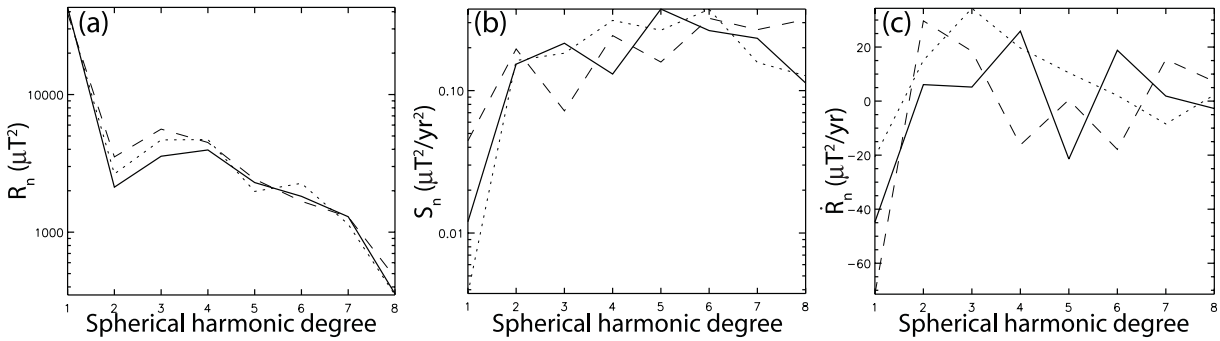

Figure 2. Three arbitrary snapshots (solid: 1900, dotted: 1940, dashed: 1980) of geomagnetic spectra from *gufm1* (Jackson *et al.* 2000) as a function of spherical harmonic degree: (a) R_n in $\mu\mathrm{T}^2$ in log-scale; (b) S_n in $\mu\mathrm{T}^2\,\mathrm{yr}^{-2}$ in log-scale; (c) $\dot{R}_n$ in $\mu\mathrm{T}^2\,\mathrm{yr}^{-1}$ in linear scale.

$n_{\max} = 8$ to avoid biases due to variations in data quality and spatial resolution with time (Holme *et al.* 2011). Fig. 2(a) demonstrates the well-known dipole-dominated geomagnetic field spectrum with decreasing power towards higher harmonics. The SV spectrum in Fig. 2(b), in contrast, is increasing with n, so the dipole SV contains less energy than the SV in the higher harmonics. The rate of change of the dipole energy $\dot{R}_1$ is negative (Fig. 2c), reflecting the historical decrease in dipole intensity (Gubbins 1987; Olson & Amit 2006). Interestingly, although the energy in the dipole change is smaller than in the higher harmonics, that is, $S_1 < S_{n\neq 1}$, the rate of change of the dipole energy is in most periods the largest, that is, $|\dot{R}_1| > |\dot{R}_{n\neq 1}|$. In most cases $\dot{R}_{n\neq 1}$ are positive, representing the non-dipole increase that accompanies the historical dipole decrease (Amit & Olson 2010).

For incompressible flow, the radial component of the induction equation just below the CMB where the radial velocity vanishes is

$$\dot{B}_r + \vec{u_h} \cdot \nabla B_r + B_r \nabla_h \cdot \vec{u_h} = \eta \hat{r} \cdot \nabla^2 \vec{B}, \tag{6}$$

where $\dot{B}_r$ is the time derivative of the radial magnetic field on the CMB, $\vec{u_h}$ is the free stream tangential fluid velocity vector at the top of the core, η is the magnetic diffusivity of the outer core, $\hat{r}$ is the radial unit vector and $\vec{B}$ is the magnetic field vector. The subscript h denotes the direction tangent to the spherical CMB surface: $\nabla_h = \nabla - \frac{\partial}{\partial r}$.

Assuming that magnetic diffusion is negligible with respect to magnetic field advection by the flow (Roberts & Scott 1965), (6) becomes

$$\dot{B}_r = -(\vec{u_h} \cdot \nabla B_r + B_r \nabla_h \cdot \vec{u_h}). \tag{7}$$

Amit & Olson (2010) have shown that the radial magnetic induction equation can be recasted to a time-evolution equation for the magnetic energy spectrum. In the frozen-flux limit, their eq. (8) is simply

$$\dot{R}_n = T_n, \tag{8}$$

where T_n is the transfer spectrum representing magnetic energy transfer induced by the flow.

The tangential fluid velocity at the top of the core can generally be written as

$$\vec{u_h} = \nabla \times \mathcal{T} \hat{r} + \nabla_h \mathcal{P}, \tag{9}$$

where $\mathcal{T}$ and $\mathcal{P}$ are toroidal and poloidal flow potentials, respectively. The tangential flow components are then given by

$$u_\phi = -\frac{1}{r}\frac{\partial \mathcal{T}}{\partial \theta} + \frac{1}{r \sin\theta}\frac{\partial \mathcal{P}}{\partial \phi}, \tag{10}$$

$$u_\theta = \frac{1}{r \sin\theta}\frac{\partial \mathcal{T}}{\partial \phi} + \frac{1}{r}\frac{\partial \mathcal{P}}{\partial \theta}, \tag{11}$$

where r, θ, ϕ are the radial, co-latitude and longitude spherical coordinates. Eq. (7) can be written in terms of $\mathcal{T}$ and $\mathcal{P}$ as

$$\dot{B}_r = -\left[\frac{1}{r^2 \sin\theta}\left(\frac{\partial \mathcal{T}}{\partial \phi}\frac{\partial B_r}{\partial \theta} - \frac{\partial \mathcal{T}}{\partial \theta}\frac{\partial B_r}{\partial \phi}\right) + \frac{1}{r^2}\left(\frac{\partial \mathcal{P}}{\partial \theta}\frac{\partial B_r}{\partial \theta} + \frac{1}{\sin^2\theta}\frac{\partial \mathcal{P}}{\partial \phi}\frac{\partial B_r}{\partial \phi}\right) + B_r \nabla_h^2 \mathcal{P}\right]. \tag{12}$$

We consider two types of flows. First, synthetic flows are constructed from single spherical harmonics as $\mathcal{T} = A\mathcal{T}_n^{mc}$ or $\mathcal{T} = A\mathcal{T}_n^{ms}$, where A is the flow amplitude, $\mathcal{T}_n^m$ is the associated Legendre polynomial and the superscripts c and s denote $\cos m\phi$ and $\sin m\phi$, respectively. The same nomenclature applies for the poloidal potential, $\mathcal{P} = A\mathcal{P}_n^{mc}$ or $\mathcal{P} = A\mathcal{P}_n^{ms}$. In all cases, we tune A so that the maximum flow is arbitrarily set to 10 km yr^{-1}, allowing comparison between the efficiency of different synthetic flows to generate T_n. We use the field at 1980 from the historical model *gufm1* (Fig. 3) for comparing the behaviour of energy transfer produced by different synthetic flows.

Secondly, frozen-flux core flow models inferred from inversions of geomagnetic SV data are investigated. We use the helical core flow model of Amit & Olson (2004), which assumes a linear relation between the tangential flow divergence $\nabla_h \cdot \vec{u_h}$ and the radial vorticity ζ at the top of the free stream

$$\nabla_h \cdot \vec{u_h} = \mp k\zeta, \tag{13}$$

where the minus/plus signs apply in the northern/southern hemispheres, respectively, and k is a constant. We choose flow models obtained with $k = 0.15$ that was found to optimize the agreement with the observed length of day variation record (Amit & Olson 2006). As described in Amit & Olson (2004), the toroidal and poloidal flow potentials were computed from a set of advection–diffusion equations based on (12) and (13) and solved on a regular spherical grid. Single epoch flows between 1840 and 1990 in 5 yr intervals were inverted based on the historical geomagnetic SV model from *gufm1*. Here, the field models of the respective periods are used. We note that the local numerical scheme used to infer the core flow models does not impose any spectral constraint (Amit & Olson 2004).

To calculate magnetic energy transfer from one degree to another, we track the interactions between each spherical harmonic degree n' of the radial field with the full flow $\vec{u_h}$. The total radial field on

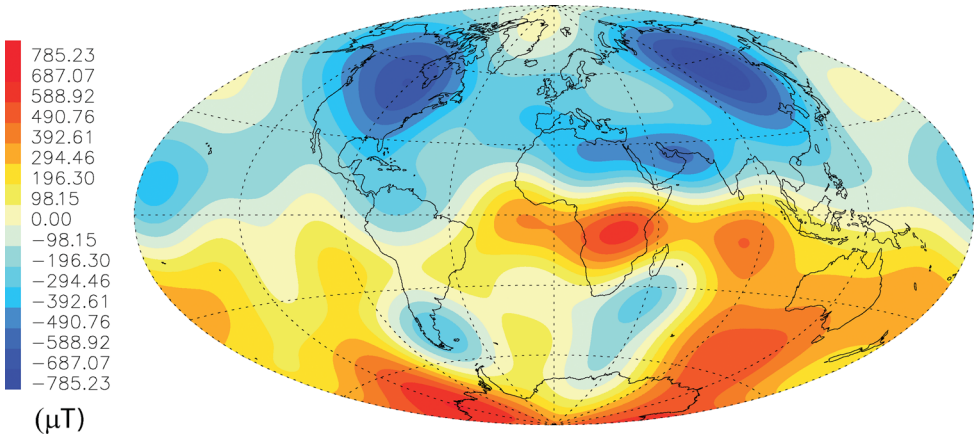

Figure 3. The radial geomagnetic field on the CMB in μT in 1980 from *gufm1* (Jackson *et al.* 2000) truncated at spherical harmonic degree $n_{\max} = 8$.

the CMB is given in terms of the Gauss coefficients by

$$B_{\rm r} = \sum_{n=1}^{n_{\max}} \sum_{m=0}^{n} \left(\frac{a}{c}\right)^{n+2} (n+1)\, P_n^m(\cos\theta) \left(g_n^m \cos m\phi + h_n^m \sin m\phi\right), \tag{14}$$

where P_n^m are the Schmidt semi-normalized Legendre polynomials. We calculate the contribution to $\dot{B}_{\rm r}$ from the advection of the radial field of degree n' $B_{\rm r}^{n'}$ by the flow $\vec{u_h}$ using the frozen-flux radial magnetic induction eq. (12). Note that this interaction in general may contain all spherical harmonics. We then apply a spectral transform to obtain the SV Gauss coefficients $\dot{g}_n^m$ and $\dot{h}_n^m$, and in conjunction with the field Gauss coefficients g_n^m and h_n^m we compute the energy transfer based on (4) and (8). We denote as $T_{n'\to n}$ the energy change of degree n due to the interaction of the degree n' field $B_{\rm r}^{n'}$ with the total flow $\vec{u_h}$. The net energy transfer between degrees p and n is the matrix component

$$T_{pn} = T_{p\to n} - T_{n\to p}, \tag{15}$$

where $p < n$. The physical meaning of (15) is that energy may be transferred from degree p to degree n and vice versa, and the net balance is the difference between the two transfers. If T_{pn} is positive net energy is transferred from the lower degree p to the higher degree n, whereas if T_{pn} is negative net energy is transferred from the higher degree n to the lower degree p. The matrix T_{pn} therefore contains only the terms above the main diagonal, because the terms below the main diagonal are folded into the net transfer, and the main diagonal itself represents energy transfer within a degree (e.g. from the axial to the equatorial dipole). Local transfer is represented by the diagonal just above the main diagonal in T_{pn} (i.e. $n = p+1$). To assess the role of non-local transfer, we calculate the ratio of absolute local to non-local transfers

$$L = \frac{\sum_{n'=1}^{n_{\max}-1} |T_{n'n'+1}|}{\sum_{p'=1}^{n_{\max}-2} \sum_{n'=p'+2}^{n_{\max}} |T_{p'n'}|}. \tag{16}$$

We repeat these calculations for all degrees from $n = 1$ to $n_{\max}$. Apart from the matrix T_{pn}, we also calculate the integrated magnetic energy change by advection for each degree strictly due to transfer within the observed spectrum $n_{\max} \geq n \geq 1$, from hereafter denoted by $T_n(\mathbb{N}_1^{\max})$, as

$$T_n\left(\mathbb{N}_1^{\max}\right) = \sum_{n'=1}^{n-1} T_{n'n} - \sum_{n'=n+1}^{n_{\max}} T_{nn'}. \tag{17}$$

Finally, we also compute the overall change following (4) by calculating the SV from the interaction of the full field $B_{\rm r}$ with the full flow, from hereafter denoted by $T_n(\mathbb{N}_1^{\max} \to \mathbb{N}_1)$, that is, energy transfer from the observed spectrum $\mathbb{N}_1^{\max}$ to the entire spectrum $\mathbb{N}_1$. Note that the latter includes energy leaking from $n \leq n_{\max}$ to $n > n_{\max}$, whereas T_{pn} and $T_n(\mathbb{N}_1^{\max})$ contain strictly energy transfers within $n \leq n_{\max}$.

For all forward calculations of the radial frozen-flux magnetic induction equation we use a spatial grid step of 5°. The spectral transforms are performed until degree and order 10, but we consider only degrees $n = 1$–8 from which the core field model was constructed. To test the precision of our numerical scheme, we first consider two simple synthetic flows. In case 1 (see Table 1), solid body rotation with respect to the rotation axis $\mathcal{T}_1^0$ uniformly advects the field to the west. The SV contains azimuthal phase variations only, so the power in each degree is unchanged. This can easily be demonstrated analytically. For example, substituting $\mathcal{T} = A\mathcal{T}_1^0$ and a dipole field into (12) gives

$$\dot{B}_{\rm r} = -\left(\frac{2A}{c^2}\right)\left(\frac{a}{c}\right)^3 \left(-g_1^1 \sin\theta \sin\phi + h_1^1 \sin\theta \cos\phi\right). \tag{18}$$

Table 1. Summary of synthetic flows. Horizontal line spaces separate tests, symmetric flows and antisymmetric flows. The integrated dipole energy change by advective transfers within the observed spectrum is $T_1(\mathbb{N}_1^8)$, and the rms absolute integrated change induced by the flow within the observed spectrum based on (5) is $\sum_1^8 \frac{n+1}{2n+1} |T_n(\mathbb{N}_1^8)|$, both in $\mu\mathrm{T}^2\,\mathrm{yr}^{-1}$. The difference between harmonics participating in the dominant transfers is Δn.

Case	Synthetic flow	$T_1\left(\mathbb{N}_1^8\right)$	$\sum_1^8 \frac{n+1}{2n+1} \lvert T_n\left(\mathbb{N}_1^8\right)\rvert$	Δn
1	$\mathcal{T}_1^0$	0.0006	0.015	0
2	$\mathcal{T}_1^{1c}$	1.54	3.85	0
3	$\mathcal{P}_2^0$	204.40	426.75	2
4	$\mathcal{T}_2^{1c}$	83.76	210.82	1
5	$\mathcal{P}_2^{2c}$	155.60	312.28	2
6	$\mathcal{P}_2^{2s}$	34.51	179.97	2
7	$\mathcal{T}_5^{4c}$	27.26	128.20	2–4
8	$\mathcal{P}_1^0$	−88.50	366.04	1
9	$\mathcal{T}_2^0$	22.07	136.85	1

Identifying the spherical harmonics in (18) indicates that the SV in this case is comprised of equatorial dipole changes only: $\dot{g}_1^1 = -\frac{A}{c^2} h_1^1$, $\dot{h}_1^1 = \frac{A}{c^2} g_1^1$, and therefore (4) and (8) give $T_1 = 4(\frac{a}{c})^6 (g_1^1 \dot{g}_1^1 + h_1^1 \dot{h}_1^1) = 0$. In words, energy has exchanged hands strictly between g_1^1 and h_1^1 without involving other harmonics, and the overall dipole energy is unchanged. The same type of magnetic energy exchange appears in case 2 where $\mathcal{T} = A\mathcal{T}_1^{1c}$. In this case, solid body rotation about an axis in the equatorial plane results in uniform meridional advection and energy transfer from g_1^0 to h_1^1. As in case 1, no energy transfer between different degrees occurs. These expected results can be directly obtained from the selection rules of Bullard & Gellman (1954) that restrict the interaction of a $\mathcal{T}_1^0$ flow and a poloidal magnetic field to either a change of phase in the poloidal field or to a conversion to a toroidal field (see their fig. 3c).

The known solutions in cases 1 and 2 allow testing the accuracy of our numerical scheme. In these cases the matrix components T_{np} representing the net energy transfer, the total change for each degree strictly due to energy transfer within the observed spectrum $T_n(\mathbb{N}_1^8)$ and the overall change including energy leaking from the observed spectrum to degrees beyond $n_{\max} = 8$ denoted by $T_n(\mathbb{N}_1^8 \to \mathbb{N}_1)$ are expected to be zero, so non-zero values in these quantities are numerical errors. Compared with a reference value, given in case 2 by the contribution of the term $g_1^0 \dot{g}_1^0$ to T_n, the maximum numerical error in case 2 is ∼2.2 per cent. In case 1, where the reference value is the contribution of the $g_1^1 \dot{g}_1^1$ term, the maximum numerical error is 0.2 per cent. The relative error in case 2 is larger than in case 1 because the large g_1^0 term participates in the SV in case 2 but not in case 1. Overall, simulating a zero $\dot{R}_n$ is most stringent, and is likely to yield the largest relative numerical errors. The maximal ∼2 per cent error reported here should therefore be considered as an upper bound relative error estimate.

3 RESULTS

3.1 Synthetic flows

We begin by analysing the magnetic energy transfer due to the interaction of simple synthetic single harmonic flows with the geomagnetic field. As stated earlier, we use for all synthetic flow cases the geomagnetic field model *gufm1* of Jackson *et al.* (2000) for the year 1980 expanded until spherical harmonic degree $n_{\max} = 8$. We

focus on flows symmetric to the equator that are often considered more geophysical due to the dominance of rotational effects in the Earth's core. In addition, we consider some antisymmetric flows that are suggested by some core flow models inferred from inversions of the geomagnetic SV. We note that for the synthetic flows the sign of the circulation is arbitrary; A change of sign for the flow would result in a change of sign for all components of the matrix T_{pn}, so that if flow $\mathcal{T}_n^m$ yields dipole decrease, flow $-\mathcal{T}_n^m$ would yield dipole increase. A summary of the synthetic flows and some statistics of the results are given in Table 1.

While the differential rotation in case 1 may be important for the dynamo generation, such a flow does not yield any poloidal energy transfer at the top of the core. The next equatorially symmetric toroidal flow is $\mathcal{T}_2^{1c}$ (case 4). This flow is comprised of two pairs of vortices, a cyclone and an anticyclone, in each hemisphere. The meridional flow, which is the sole component that may cause axial dipole changes (Olson & Amit 2006), is equatorward in $\phi = 90^\circ$W and poleward in $\phi = 90^\circ$E. The main SV structures are related to the meridional advection of the two intense high-latitude geomagnetic flux patches in the northern hemisphere (Fig. 4a), which are in-phase with the flow. The reduction of the axial dipole by the southward advection of the north American patch is balanced by the dipole strengthening due to the northward advection of the Siberian patch. In the southern hemisphere, the two normal flux patches yield little SV due to the weak meridional field gradient associated with the patch below the Indian Ocean and the off-phase relation with the flow of the patch below the Pacific. However, the equatorward advection of the reversed flux patch below Patagonia (Fig. 4a) results in a net dipole increase (Fig. 4c).

Our spectral transfer analysis of case 4 indicates that practically all the dipole increase is due to net energy transfer from the quadrupole (Fig. 4b), which is simultaneously decreasing (Fig. 4c). This transfer between degrees 1 and 2 can be demonstrated analytically. Substituting an axial dipole field and the $\mathcal{T}_2^{1c}$ flow into (12) gives

$$\dot{B}_\mathrm{r} = -\frac{2A}{c^2}\left(\frac{a}{c}\right)^3 g_1^0 \cos\theta \sin\theta \sin\phi. \tag{19}$$

The coefficient $\dot{h}_2^1$ arises from (19). Because $h_2^1 < 0$ and $\dot{h}_2^1 = -\frac{2\sqrt{3}A}{9c^2}(\frac{a}{c})^{-1} g_1^0 > 0$, the term $h_2^1 \dot{h}_2^1$ provides a significant negative contribution to $T_{1\to 2}$. In addition, substituting an h_2^1 field and the $\mathcal{T}_2^{1c}$ flow into (12) gives

$$\dot{B}_\mathrm{r} = \frac{6\sqrt{3}A}{5c^2}\left(\frac{a}{c}\right)^4 h_2^1 \left(5\cos^3\theta - 3\cos\theta + \frac{1}{2}\cos\theta\right). \tag{20}$$

The first two terms on the right-hand side of (20) are identified with the axial octupole SV. The last term on the right-hand side of (20) gives the coefficient $\dot{g}_1^0$. Because $g_1^0 < 0$ and $\dot{g}_1^0 = \frac{3\sqrt{3}A}{10c^2}(\frac{a}{c})h_2^1 < 0$,

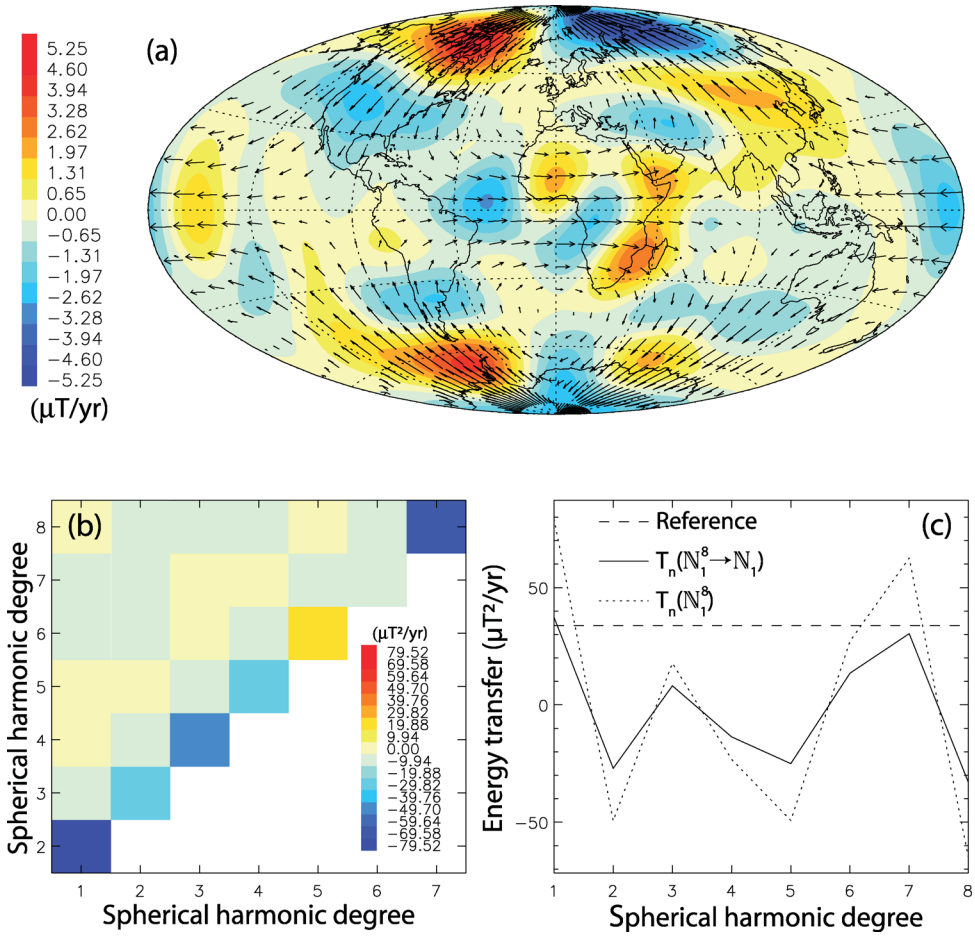

Figure 4. Case 4: (a) SV in μT yr^{-1} with superimposed arrows for the synthetic flow; (b) matrix components T_{np} in μT^2 yr^{-1}; (c) total change within the observed spectrum $T_n(\mathbb{N}_1^8)$ (dotted) and total change including energy leaking beyond $T_n(\mathbb{N}_1^8 \to \mathbb{N}_1)$ (solid), both in μT^2 yr^{-1}. The reference horizontal dashed line in (c) is the contribution of the term $g_1^0 \dot{g}_1^0$ to T_1.

the term $g_1^0 \dot{g}_1^0$ provides a significant positive contribution to $T_{2\to1}$. Both contributions, the negative $h_2^1 \dot{h}_2^1$ to $T_{1\to2}$ and the positive $g_1^0 \dot{g}_1^0$ to $T_{2\to1}$, add up to a negative T_{12} corresponding to a net energy transfer from the quadrupole to the dipole (Fig. 4b), to a dipole increase and to a quadrupole decrease (Fig. 4c).

Overall, the magnetic energy transfer is dominantly local in this case, that is, the difference between the degrees involved in the transfers is $\Delta n = 1$ (Table 1). An inverse energy cascade is seen continuously throughout almost the entire spectrum, except for forward cascade from $n = 5$ to $n = 6$. In all degrees, however, the transfer is always local between neighbouring harmonics. Moreover, the integrated energy transfer within the observed spectrum $T_n(\mathbb{N}_1^8)$ and the total advective change $T_n(\mathbb{N}_1^8 \to \mathbb{N}_1)$ are well correlated (Fig. 4c), so the energy leaking out of the observed spectrum plays a secondary role in the large-scale kinematics.

The largest scale symmetric flows that generate kinematic dynamos were found based on linear combinations of $\mathcal{T}_1^0$, $\mathcal{P}_2^0$, $\mathcal{P}_2^{2c}$ and $\mathcal{P}_2^{2s}$ (Kumar & Roberts 1975; Gubbins *et al.* 2000a,b). The poloidal flow $\mathcal{P}_2^{2c}$ of case 5 is comprised of two equatorial sources and two equatorial sinks, with saddles in the poles. The meridional flow at 90°E and 90°W (the longitudes of the equatorial sources) advects the two northern hemisphere high-latitude intense flux patches poleward (see the two large positive SV structures in Fig. 5a), thus strengthening the axial dipole (Fig. 5c). This dipole increase is due to energy transfer from degree 3 (Fig. 5b). Substituting an axial dipole field and the $\mathcal{P}_2^{2c}$ flow into (12) gives

$$\dot{B}_r = \frac{20A}{c^2}\left(\frac{a}{c}\right)^3 g_1^0 \sin^2\theta \cos\theta \cos 2\phi \qquad (21)$$

demonstrating that the SV due to such a field–flow interaction indeed results in a strong degree 3 coefficient $\dot{g}_3^2$. Changing the phase of the flow may be important. The $\mathcal{P}_2^{2s}$ flow is off-phase with the northern hemisphere normal flux patches resulting in bipolar SV structures due to westward drift that does not affect the axial dipole. In the southern hemisphere the distance between the two normal flux patches is such that one patch is advected poleward while the other is advected equatorward, resulting in a weak net dipole change (Table 1). In both cases 5 and 6, the energy transfer is strictly between harmonics differing by $\Delta n = 2$, in agreement with the selection rules of the Gaunt and Elsasser integrals (see fig. 5c of Bullard & Gellman 1954). In case 5, the largest net energy transfer is from $n = 3$ to the dipole (Figs 5b and c); In case 6, the energy is transported forward from degrees 3, 4 and 5 to degrees 5, 6 and 7, respectively, resulting in a minimum in T_3 and a maximum in T_7 (not shown). Also note that in both cases the dipole increases when accounting for energy transfer strictly within the observed spectrum, but the dipole change is much smaller when including the energy escaping from the observed spectrum to higher degrees.

To investigate the impact of small scales on the magnetic energy transfer, we consider case 7 with a toroidal $\mathcal{T}_5^{4c}$ flow. The resulting SV is characterized by somewhat smaller scales than in the previous cases (Fig. 6a). More importantly, the transfer is less local, and the difference between the harmonics involved in the transfer is not

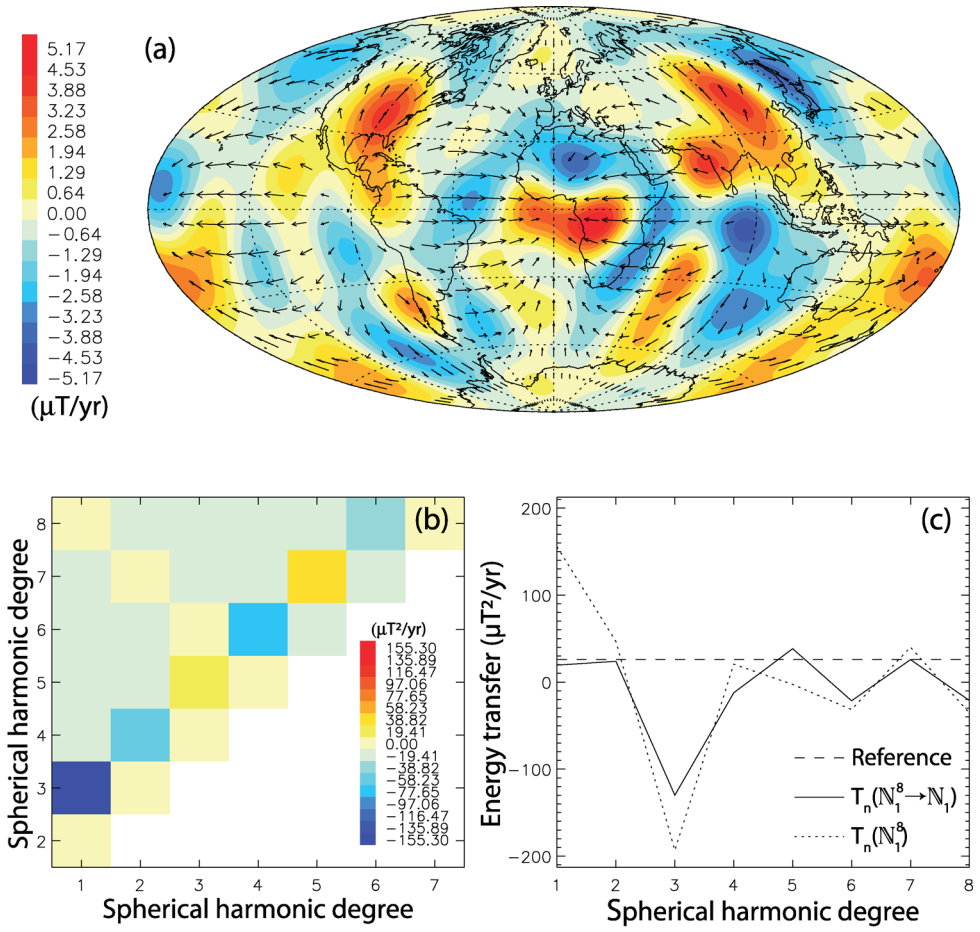

Figure 5. As in Fig. 4 for case 5.

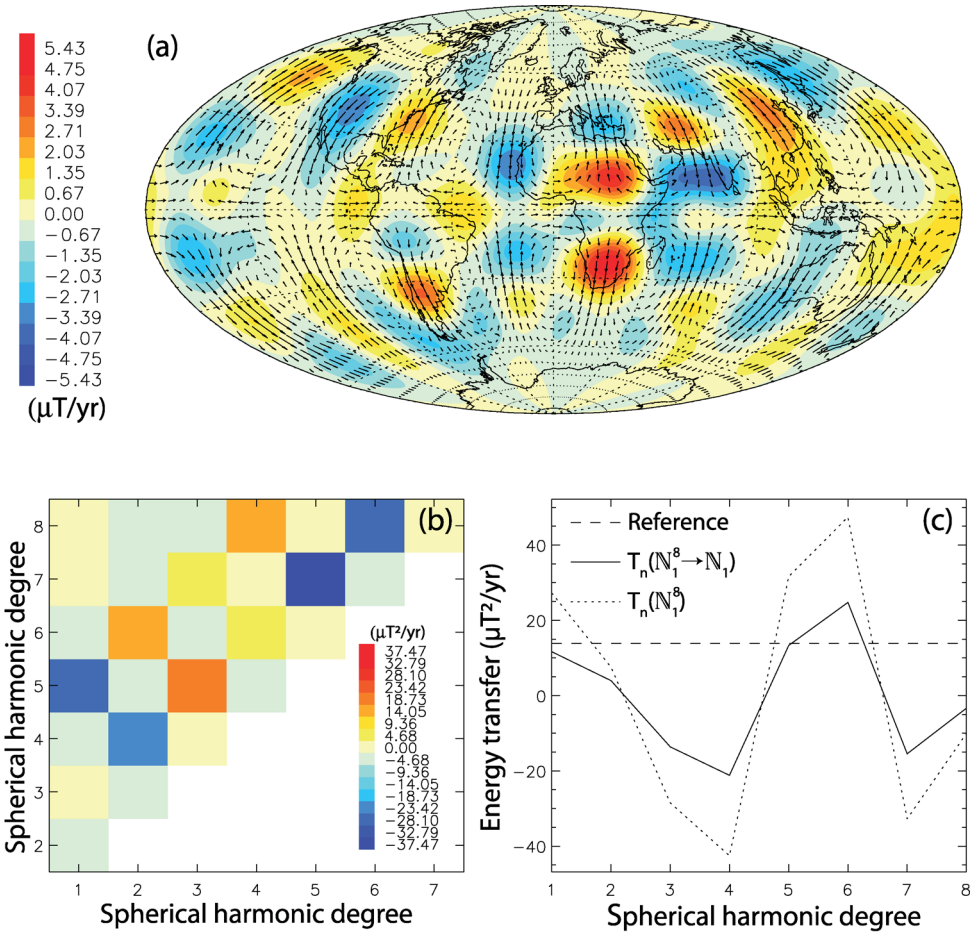

Figure 6. As in Fig. 4 for case 7.

fixed, ranging $\Delta n = 2$–4. The most significant energy transfer is from $n = 7$ to $n = 5$ (Fig. 6b), resulting in a minimum in T_7 (Fig. 6c).

We also examine two antisymmetric flows, one toroidal and one poloidal (see Table 1). The poloidal flow $\mathcal{P}_1^0$ of case 8 is all northward from a south pole source to a north pole sink. The transfer is purely local (Table 1), as prescribed by the selection rules that permit either poloidal-to-poloidal magnetic energy transfer between neighbouring degrees or poloidal-to-toroidal within the same degree (see fig. 4 of Bullard & Gellman 1954). The toroidal flow $\mathcal{T}_2^0$ (case 9) is zonal with a north–south shear, so that the motion is eastward/westward in the northern/southern hemispheres, respectively. In such a purely zonal motion, dipole changes are excluded to the equatorial component (Amit & Olson 2008). The energy transfer in this case is local, that is, between neighbouring harmonics (Fig. 7b). An inverse magnetic energy cascade appears from degree $n = 4$ to the dipole and from degree $n = 7$ to $n = 5$, with the exception of a forward transfer from degree $n = 4$ to $n = 5$, resulting in a minimum in T_4 (Fig. 7c).

3.2 Core flows

We now implement our formalism to calculate the geomagnetic energy transfer induced by core flow models. As stated earlier, we use the purely helical core flow model of Amit & Olson (2004) obtained from inversions of geomagnetic SV from *gufm1* (Jackson *et al.* 2000) in 5-yr intervals during the period 1840–1990. In addition to the two integrated quantities, one of magnetic energy transfer strictly within the observed spectrum $T_n(\mathbb{N}_1^8)$, and the other of magnetic energy transfer from the observed to the entire spectrum $T_n(\mathbb{N}_1^8 \rightarrow \mathbb{N}_1)$, we also consider the observed change $\dot{R}_n$ calculated based on the geomagnetic field and SV Gauss coefficients (red solid line in Fig. 8). The observed $\dot{R}_n$ differs from T_n because the latter is affected by the SV misfit of the core flow models. In addition, magnetic diffusion is likely to affect $\dot{R}_n$ (Holme & Olsen 2006; Holme 2007; Amit & Christensen 2008). In contrast, it is possible that inverted core flows cannot mimic magnetic diffusion (Holme 2007), and unmodelled diffusive effects are absorbed by the SV misfit (Rau *et al.* 2000). If this is indeed the case, our calculated transfer spectrum T_n may indeed represent the transport of energy by the flow.

Fig. 8 shows the temporal evolution of the three quantities for each spherical harmonic degree. Overall, the three quantities follow similar trends, suggesting that the geomagnetic energy leakage outside the observed spectrum, the energy change due to interactions of small-scale flow with large-scale field and of small-scale field with large-scale flow, the SV misfit of the core flow models and the impact of magnetic diffusion on the shape of the geomagnetic field spectrum, are all secondary in the interpretation of the geomagnetic energy transfer. The largest discrepancies among the three curves seem to appear in the dipole term. In addition, the dipole change curve contains higher frequencies than the higher harmonics, highlighting the challenging task of investigating dipole

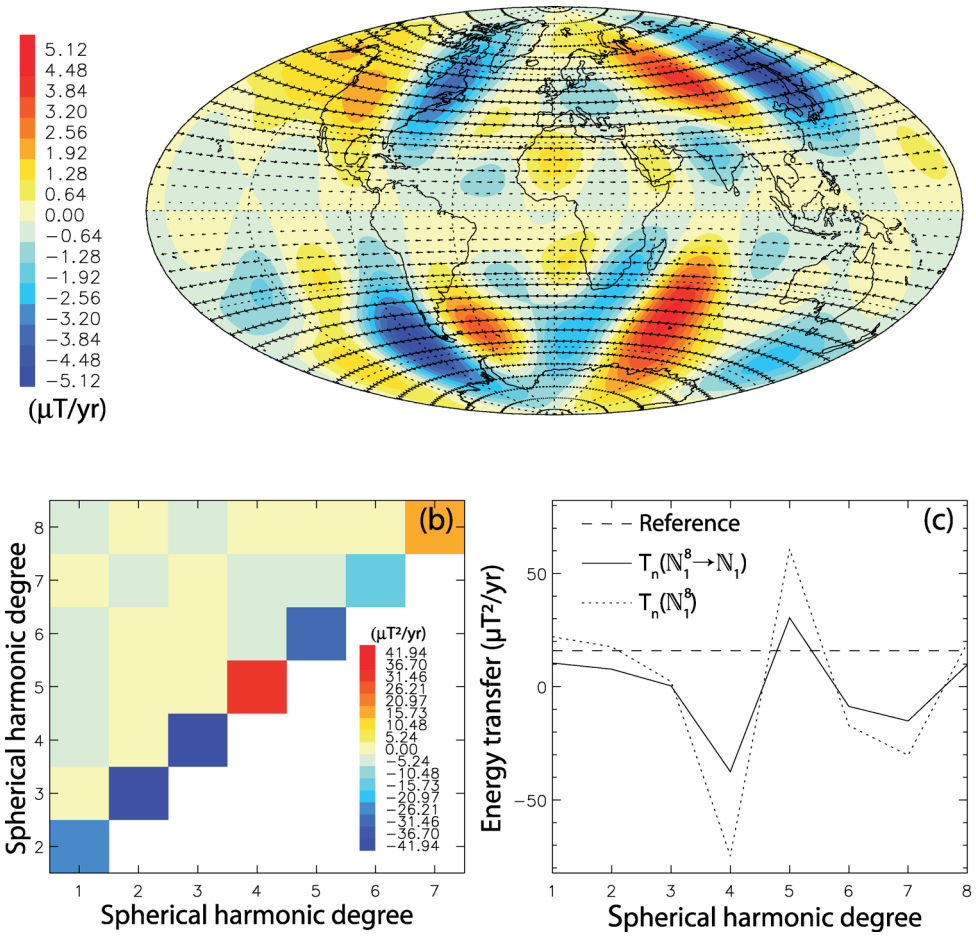

Figure 7. As in Fig. 4 for case 9. The reference horizontal dashed line in (c) is the contribution of the term $h_1^1 \dot{h}_1^1$ to T_1.

variability. The quadrupole energy rate of change is the smallest in magnitude. Higher harmonics often display relatively long periods of either steady or linear trends, possibly due to the stronger temporal regularization of higher degrees in *gufm1*.

As shown in the movie *TransferGeomag.gif* and reported in Table 2, a pattern of alternating minima/maxima is a robust feature of the transfer spectra T_n induced by the core flows. The period 1840–1910 is characterized by even maxima and odd minima T_n, whereas the period 1955–1990 is reversed with odd maxima and even minima. The intermediate period is transitory with a relatively smooth T_n pattern. Overall, the analysis of the core flows is much more complex than in the synthetic flows. Energy transfer occurs both locally and between non-neighbouring degrees. The ratio of local to non-local transfers is about ∼0.5 (Table 2). Cascades are not continuous through long parts of the spectrum, but instead energy transfer in one direction is often interrupted by opposite direction of transport between neighbouring degrees. Most strikingly, rapid variations in T_{pn} from one snapshot to another provide evidence for the strong time-dependence of core dynamics on short timescales.

Kolmogorov-like turbulent behaviour may arise in a statistical sense (Moffatt 1978), so it is worth-while examining the time-average energy transfer. Following Amit & Olson (2010), we search for time-averages of intervals that may highlight some trends in the behaviour of the energy transfer. Figs 9–11 show three time-averages of intervals characterized by different T_n trends (see Fig. 8 and Table 2). In the time-average of the period 1840–1910, even maxima and odd minima dominate T_n at intermediate degrees (Fig. 9b). The lowest diagonal ($\Delta n = 1$) is mostly negative (Fig. 9a), that is, an inverse cascade transfers geomagnetic energy from high to low neighbouring degrees. The left column, in contrast, is characterized by positive structures, representing forward non-local transfer from the dipole mainly to degrees $n = 3$–4 and $n = 6$ (Fig. 9a) that results in the two peaks of T_4 and T_6 (Fig. 9b).

In 1915–1950, both the lowest diagonal and the left column contain significant positive structures, so energy cascades forward through neighbouring degrees, but also energy is transferred from the dipole to higher degrees $n = 3$ and 5. The spectral region in between the lowest diagonal and left column contains some negative values, mostly due to energy transfer from $n = 5$ to $n = 2$–3 (Fig. 10a). Overall, the forward energy transfer in both the lowest diagonal and the left column yield simultaneous dipole decrease and non-dipole increase at this interval (Figs 10b and 8).

In the interval 1955–1990, the upper part of the transfer matrix is dominantly positive, the intermediate is mostly negative and the lower is once again positive (Fig. 11a). Geomagnetic energy is transported from most of the spectrum to the high degrees, especially to $n = 7$. Energy leaves from intermediate degrees $n = 4$–6 to the rest of the spectrum. Dipole energy is transferred to degrees 2–3. The total transfer contains maxima in odd degrees and minima in even degrees (Fig. 11b).

Finally, we wish to relate the spectral analysis with its origin in physical space. Holme *et al.* (2011) demonstrated that field

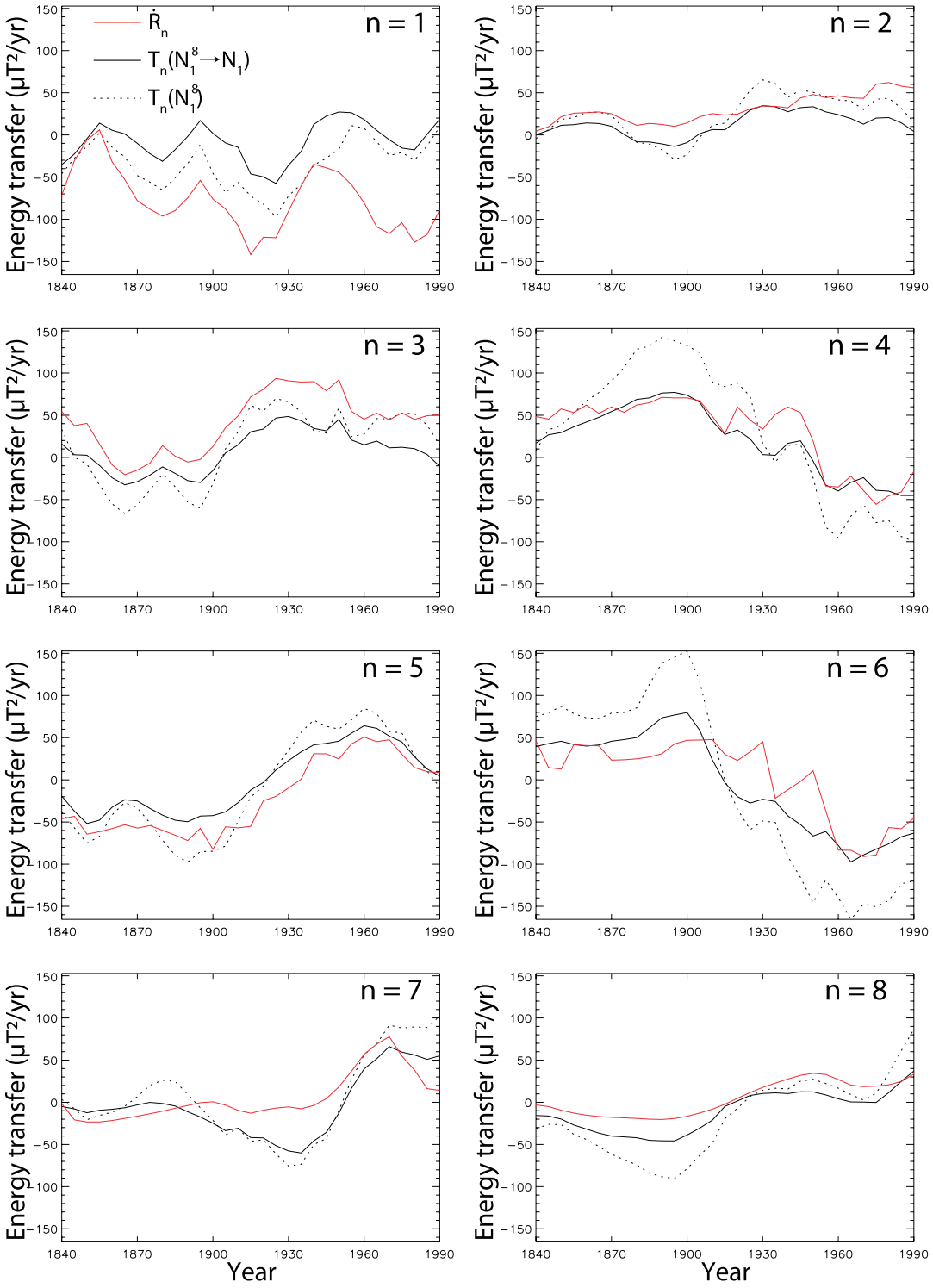

Figure 8. Total geomagnetic energy transfers $T_n(\mathbb{N}_1^8)$ (dotted black) and $T_n(\mathbb{N}_1^8 \rightarrow \mathbb{N}_1)$ (solid black), and the observed change $\dot{R}_n$ (red), for each spherical harmonic degree as a function of time for the historical period 1840–1990.

concentration in one hemisphere (eastern or western) corresponds to a spectrum dominated by even harmonics. The geomagnetic SV exhibits strong hemispheric dichotomy between the active Atlantic and the quite Pacific, which is thought to originate in thermal core–mantle coupling (Christensen & Olson 2003; Gubbins 2003). The product of B_r and SV, which is relevant for $\dot{R}_n$ (4), has roughly the same hemispheric asymmetry, but with an opposite sign (because g_1^0 is negative). This is evident in the coincidence between minima of S_n and maxima of $\dot{R}_n$ and vice versa (Figs 2b and c). The alternating even/odd peaks of T_n are therefore partially related to the Atlantic/Pacific SV dichotomy. However, the strong temporal evolution of T_n seen in Figs 9–11 indicates that thermal core–mantle coupling alone cannot explain the observed spectral variations.

Table 2. Summary of core flows in 5-yr intervals for the period 1840–1990. The integrated dipole energy change by transfers within the observed spectrum is $T_1(\mathbb{N}_1^8)$, and the rms absolute integrated change within the observed spectrum based on (5) is $\sum_1^8 \frac{n+1}{2n+1}|T_n(\mathbb{N}_1^8)|$, both in $\mu\mathrm{T}^2\,\mathrm{yr}^{-1}$. Even maxima and odd minima in $T_n(\mathbb{N}_1^8)$ are denoted by 'Even/odd', odd maxima and even minima are denoted by 'Odd/even', and '–' marks a relatively smooth pattern. The ratio of local to non-local transfers L (16) is also given. Horizontal line spaces separate the different Max/Min periods. The statistics of the total and partial time-averages are given at the bottom.

Year	$T_1\left(\mathbb{N}_1^8\right)$	$\sum_1^8 \frac{n+1}{2n+1}\lvert T_n\left(\mathbb{N}_1^8\right)\rvert$	Max/Min	L
1840	−46.01	136.34	Even/odd	0.52
1845	−27.85	132.19	Even/odd	0.39
1850	−13.45	158.36	Even/odd	0.47
1855	2.23	169.08	Even/odd	0.52
1860	−14.65	186.25	Even/odd	0.52
1865	−26.02	198.51	Even/odd	0.50
1870	−48.15	225.36	Even/odd	0.48
1875	−55.94	240.64	Even/odd	0.46
1880	−65.47	269.47	Even/odd	0.50
1885	−50.93	300.89	Even/odd	0.53
1890	−33.99	322.07	Even/odd	0.55
1895	−11.48	312.35	Even/odd	0.55
1900	−45.57	317.63	Even/odd	0.45
1905	−68.51	281.67	Even/odd	0.34
1910	−56.29	209.10	Even/odd	0.25
1915	−72.41	185.10	–	0.32
1920	−82.05	204.77	–	0.30
1925	−97.04	252.99	–	0.39
1930	−72.24	227.27	–	0.43
1935	−58.48	215.80	–	0.55
1940	−35.87	199.43	–	0.70
1945	−27.58	208.49	–	0.68
1950	−16.92	219.63	Odd/even	0.70
1955	11.03	223.50	Odd/even	0.52
1960	8.01	259.52	Odd/even	0.37
1965	−8.15	268.37	Odd/even	0.39
1970	−24.35	251.92	Odd/even	0.47
1975	−20.92	276.11	Odd/even	0.29
1980	−29.85	275.40	Odd/even	0.30
1985	−13.05	253.39	Odd/even	0.43
1990	9.65	249.02	Odd/even	0.38
1840–1990	−35.24	81.82	–	0.46
1840–1910	−37.47	210.62	Even/odd	0.47
1915–1950	−57.82	202.69	–	0.51
1955–1990	−8.45	251.17	Odd/even	0.39

4 DISCUSSION

The analysis of the energy transfer in the synthetic flows shows that most energy transfers align on one diagonal, so the difference between dominant harmonics participating in the transfer Δn is nearly constant. Flows $\mathcal{T}_2^m$ and $\mathcal{P}_1^m$ are local, that is, energy is being transferred strictly between neighbouring harmonics and T_{pn} is dominated by the lower diagonal (see $\Delta n = 1$ in Table 1). Poloidal symmetric flows $\mathcal{P}_2^m$ that were found efficient in generating dynamo action (Kumar & Roberts 1975; Gubbins *et al.* 2000a,b) are characterized by $\Delta n = 2$. Similar energy transfer was found in the analysis of the magnetic spectrum of a numerical dynamo model (Olson *et al.* 2009). The magnetic energy transfers obtained by these low degree synthetic flows are in agreement with the selection rules of the Gaunt and Elsasser integrals (Bullard & Gellman 1954), thus confirming the sensibility of our mathematical formulation and numerical scheme. The small-scale flow $\mathcal{T}_5^{4c}$ shows deviations from a constant Δn and includes transfers between 2–4 degrees differences. Overall, the transfer induced by large-scale toroidal flows is more local than that generated by small-scale poloidal flows, in agreement with studies of MHD turbulence simulations that attributed local transfer to magnetic field advection and non-local effects to magnetic field stretching (Alexakis *et al.* 2007). Some single harmonic synthetic flows show magnetic energy cascade over most of the observed spectrum (Fig. 4).

Of the nine synthetic flows studied here, the two axisymmetric poloidal flows seem to be the most efficient in producing energy transfer in general and dipole changes in particular (Table 1). The $\mathcal{P}_2^0$ flow (case 3) has an equatorial source and polar sinks, so magnetic flux is advected from low- to high-latitudes and thus strengthening the axial dipole. Note that by simply changing the sign of the flow the opposite effect, in this case dipole decrease, is obtained. A Y_2^0 CMB heat flux heterogeneity was found to be very efficient in terms of increasing (or decreasing, depending on the sign) reversal frequency by attracting magnetic flux to the equatorial region and hence initiating dipole polarity transitions (Glatzmaier *et al.* 1999; Kutzner & Christensen 2004; Olson *et al.* 2010). Our results therefore support the importance of the $\mathcal{P}_2^0$ flow in obtaining rapid dipole changes. The axisymmetric poloidal $\mathcal{P}_1^0$ flow is perpendicular to the equator, an unlikely feature in a rapidly rotating system as the Earth's core, so it is not geophysically relevant. This flow does not change the dipole dramatically, but the energy transfer of other degrees is large.

The phase of the flow may be very important for the energy transfer. Flows $\mathcal{P}_2^{2c}$ and $\mathcal{P}_2^{2s}$ interact differently with the present geomagnetic field, resulting in remarkably different energy transfers. Flow $\mathcal{P}_2^{2c}$ is in-phase with the field in the northern hemisphere, advecting the two northern hemisphere high-latitude intense flux patches poleward and thus strengthening the axial dipole (Fig. 5c) and causing overall strong energy transfers (Table 1). In contrast, flow $\mathcal{P}_2^{2s}$ interacts with the southern hemisphere flux patches, but one patch is advected poleward while the other is advected equatorward, resulting in a weak dipole change and weaker energy transfers (Table 1). A CMB heat flux pattern of Y_2^2 was found to be inefficient in reversing the dipole (Olson *et al.* 2010), perhaps because in a dynamically self-consistent system the vortices tend to correlate with magnetic flux patches and thus minimize the advection of these high-latitude features (Amit *et al.* 2010; Finlay & Amit 2011).

While toroidal flows seem less efficient than poloidal flows in inducing energy transfers, we recall that for comparison purposes all synthetic flows were set with identical amplitudes. In the Earth's core, most studies suggest that toroidal flows are much stronger than poloidal flows, possibly by about an order of magnitude (Finlay & Amit 2011). Differences of about a factor of 2–3 between the more efficient poloidal flows to the less efficient toroidal flows (Table 1) are physically insightful, but in the geophysical context these differences could thus be overshadowed by the much larger amplitude toroidal flows in the Earth's core.

Alternating minima/maxima of T_n is characteristic of turbulent magnetic energy cascades (Alexakis *et al.* 2005b). Evidence for magnetic energy cascade is suggestive in the temporal variations of the geomagnetic energy spectrum (Voorhies 2004), in particular in the form of moving peaks of successive R_n structures with time (Amit & Olson 2010). Our detailed inspection of the energy transfer between pairs of harmonics T_{pn} shows a more complex behaviour. The magnetic energy cascade in case 4 indeed contains a pattern of alternating minima/maxima of T_n (Fig. 4). However, while such a

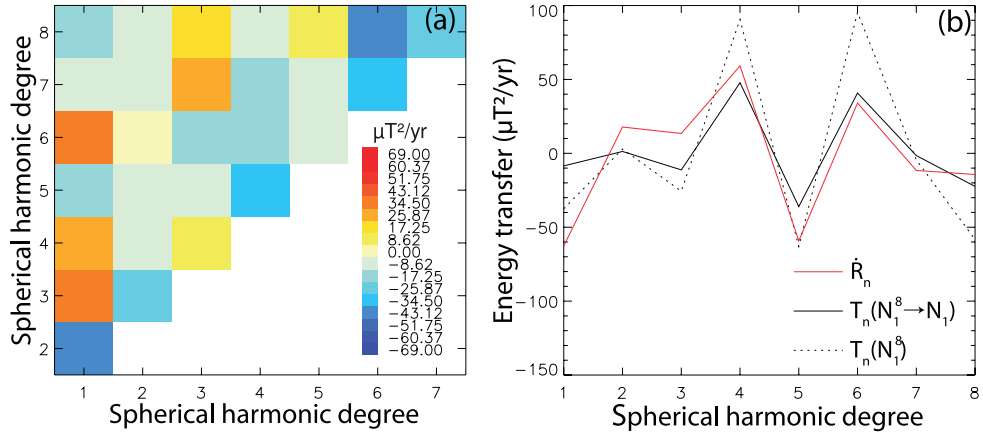

Figure 9. Geomagnetic energy transfer matrix T_{pn}, the two total energy transfers $T_n(\mathbb{N}_1^8)$ (dotted black) and $T_n(\mathbb{N}_1^8 \rightarrow \mathbb{N}_1)$ (solid black), and the observed $\dot{R}_n$ (red), all in $\mu T^2\ yr^{-1}$, for the time-average of the interval 1840–1910.

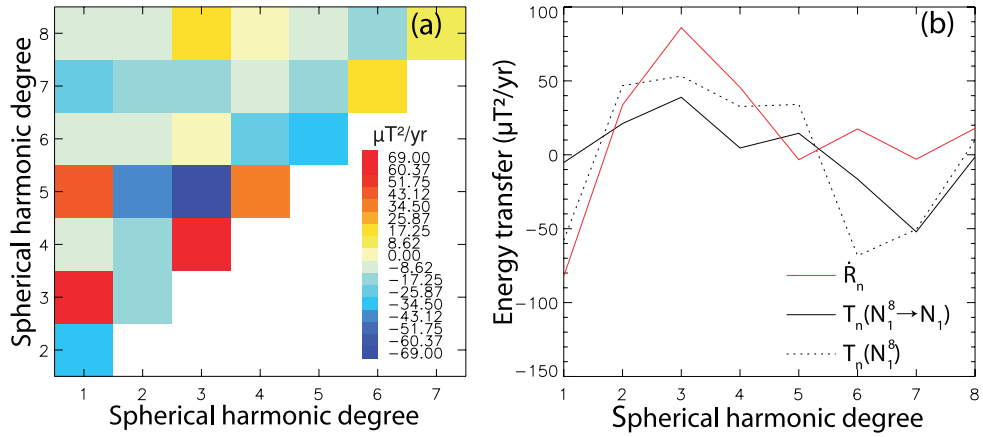

Figure 10. As in Fig. 9 for the time-average of the interval 1915–1950.

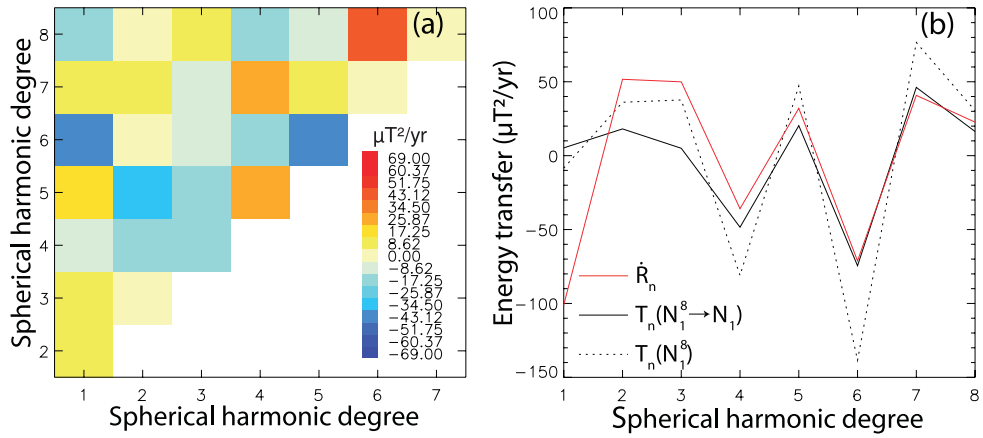

Figure 11. As in Fig. 9 for the time-average of the interval 1955–1990.

pattern of alternating minima/maxima of T_n dominates most of the core flows, the energy transfer T_{pn} is not exclusively local. In the period 1840–1910 (Fig. 9a), an inverse cascade transfers energy from high to low degrees, but in addition non-local energy transfer occurs from the dipole to higher degrees. These opposing trends result in a relatively slow dipole decrease (see minimum in Fig. 1b during this period). Energy transfer from the dipole induces maxima of T_4 and T_6, while inverse energy cascade from $n = 5$ to $n = 4$ gives a minimum at $n = 5$, thus resulting in the even maxima and odd minima T_n pattern (Fig. 9b). In the period 1955–1990 (Fig. 11a) this T_n pattern has reversed. Magnetic energy is transferred from intermediate degrees $4 - 6$ to lower and higher degrees, yielding maxima in T_5 and T_7 and minima in T_4 and T_6 (Fig. 11b). In between, a short transition period between 1915 and 1950 is characterized by a relatively smooth T_n spectrum (Fig. 10b). This transition period exhibits a forward energy cascade and non-local energy transfer from the dipole to higher degrees (Fig. 10a), giving the fastest dipole decrease (Figs 1b and 8).

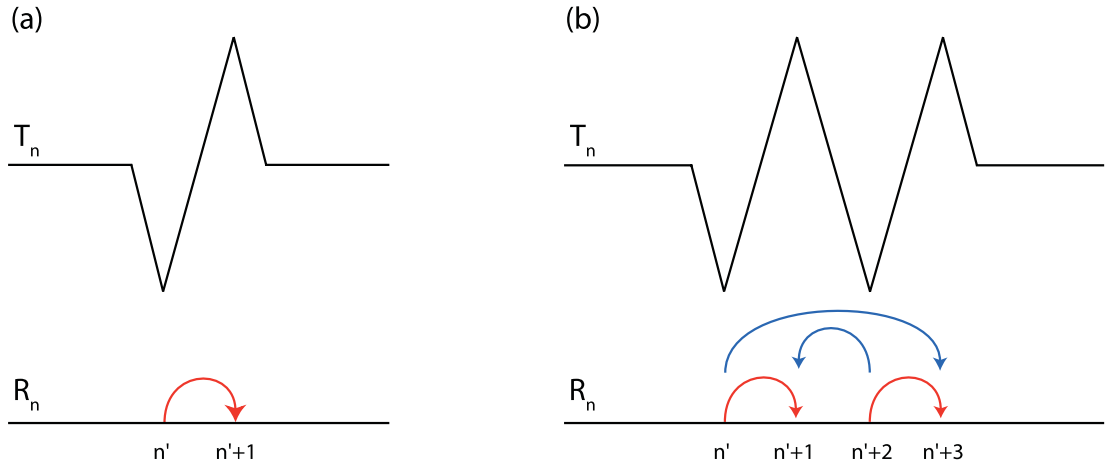

Figure 12. Schematic illustrations of alternating extrema in the transfer spectrum T_n (top) and some possible interpretations in terms of the transfer of magnetic energy spectrum R_n (bottom). (a) One pair of minimum/maximum T_n is likely to indicate local forward energy transfer. (b) Two pairs of minima/maxima T_n may be interpreted as either local forward energy cascade (red) or a more complex combination of non-local forward and local inverse transfers (blue).

The above-mentioned analysis shows that some caution is required when interpreting alternating minima/maxima T_n as an energy cascade. Indeed, when one pair of minimum/maximum appears, the most likely scenario is local transfer (see Fig. 12a following fig. 1 of Mininni 2011). However, multiple minima/maxima T_n, as typically found in the transfer spectra induced by the core flows (Figs 9 and 11), may arise due to either local or non-local transfers. In that case the solution is non-unique (Amit & Olson 2010). Consider the example in Fig. 12b where the T_n pattern contains minima in degrees n' and $n'+2$ and maxima in degrees $n'+1$ and $n'+3$. The cascade scenario would suggest forward energy transfer from n' to $n'+1$ and from $n'+2$ to $n'+3$. However, alternative scenarios are also possible, for example, non-local forward transfer from n' to $n'+3$ and local inverse transfer from $n'+2$ to $n'+1$. Tracking the transfer between each pair of degrees using the T_{pn} matrix reveals the actual paths of energy. Our T_{pn} solutions obtained from the core flows show a rich behaviour with both local Kolmogorov-like and non-local transfers.

Tracking magnetic energy transfer may shed light on the kinematics of the historical geomagnetic dipole moment decrease. Fig. 8 shows that dipole SV differs from temporal variations of higher harmonics in the larger differences among the $T_n(\mathbb{N}_1^8)$, $T_n(\mathbb{N}_1^8 \rightarrow \mathbb{N}_1)$ and $\dot{R}_n$ curves. This suggests that magnetic diffusion may play a more important role in the dipole evolution (Holme & Olsen 2006). The growth of reversed flux patches on the CMB by radial magnetic diffusion (Chulliat & Olsen 2010) has indeed been interpreted as a major cause for the dipole decrease (Gubbins 1987; Olson & Amit 2006). Dipole SV is sometimes underestimated by core flow inversions (Jackson 1997), possibly because the inversions cannot mimic the effects of magnetic diffusion SV (Whaler & Davis 1997; Holme 2007). The increasing difference between T_1 and $\dot{R}_1$ in the past several decades (Fig. 8) may suggest that dipole decrease by core flow has recently been relatively slow, and alternatively an increase in the rate of magnetic flux expulsion took place. The smaller differences among the three curves for the higher harmonics provide confidence in the overall interpretation of the energy transfer.

Amit & Olson (2010) argued that forward cascade with strong time-variability in the dipole family may explain the axial dipole decrease, while a much steadier inverse cascade governs the quadrupole family. However, their calculations rely on a local transfer assumption, which we find only partially valid. Our analysis shows that the direction of energy cascade may vary, but non-local energy transfer from the dipole to higher degrees seems more persistent. Integration over the entire observed spectrum shows that the contribution of non-local transfer is typically twice larger than that of local transfer (Table 2). Based on these findings, explaining the temporal changes in the geomagnetic spectrum by a strictly local energy transfer seems unsatisfactory.

The time-average for the entire period 1840–1990 resembles the time-average over the transitory interval 1915–1950 (Fig. 10) with both forward energy cascade from low to high degrees and non-local energy transfer from the dipole to higher degrees. The reversing trends of alternating extrema, from even maxima and odd minima between 1840 and 1910 (Fig. 9) to odd maxima and even minima between 1955 and 1990 (Fig. 11), cancel each other in the time-average of the entire period 1840–1990. It is unknown how long the first phase persisted prior to 1840. It is possible that currently the geodynamo is at the beginning of a long period of odd maxima and even minima T_n with relatively small contributions of core flow to the geomagnetic dipole decrease.

ACKNOWLEDGMENTS

HA thanks Coerte Voorhies for encouraging to test the local transfer assumption. We thank Peter Olson, Benoit Langlais, Gaël Choblet and Thierry Alboussière for insightful discussions. We are grateful to Bruce Buffett and an anonymous reviewer for constructive comments that significantly improved the paper. This study was supported by the Centre National d'Etudes Spatiales (CNES).

REFERENCES

Alexakis, A., Mininni, P. & Pouquet, A., 2005a. Imprint of large-scale flows on turbulence, *Phys. Rev. Lett.,* **93,** 264503, doi:10.1103/PhysRevLett.95.264503.

Alexakis, A., Mininni, P. & Pouquet, A., 2005b. Shell to shell energy transfer in MHD. I. steady state turbulence, *Phys. Rev. E.,* **72,** 046301, doi:10.1103/PhysRevE.72.046301.

Alexakis, A., Mininni, P. & Pouquet, A., 2007. Turbulent cascades, transfer, and scale interactions in magnetohydrodynamics, *New J. Phys.,* **9,** 1–20.

Alldredge, L., 1984. Harmonics required in main field and secular variation models, *J. Geomagn. Geoelectr.,* **36,** 63–72.

Amit, H. & Christensen, U., 2008. Accounting for magnetic diffusion in core flow inversions from geomagnetic secular variation, *Geophys. J. Int.,* **175,** 913–924.

Amit, H. & Olson, P., 2004. Helical core flow from geomagnetic secular variation, *Phys. Earth planet. Inter.,* **147,** 1–25.

Amit, H. & Olson, P., 2006. Time-average and time-dependent parts of core flow, *Phys. Earth planet. Inter.,* **155,** 120–139.

Amit, H. & Olson, P., 2008. Geomagnetic dipole tilt changes induced by core flow, *Phys. Earth planet. Inter.,* **166,** 226–238.

Amit, H. & Olson, P., 2010. A dynamo cascade interpretation of the geomagnetic dipole decrease, *Geophys. J. Int.,* **181,** 1411–1427.

Amit, H., Aubert, J. & Hulot, G., 2010. Stationary, oscillating or drifting mantle-driven geomagnetic flux patches? *J. geophys. Res.,* **115,** B07108, doi:10.1029/2009JB006542.

Aubert, J., Amit, H. & Hulot, G., 2007. Detecting thermal boundary control in surface flows from numerical dynamos, *Phys. Earth planet. Inter.,* **160,** 143–156.

Aubert, J., Aurnou, J. & Wicht, J., 2008. The magnetic structure of convection-driven numerical dynamos, *Geophys. J. Int.,* **172,** 945–956.

Batchelor, G., 1953. *The Theory of Homogeneous Turbulence,* Cambridge University Press, Cambridge, UK.

Bullard, E. & Gellman, H., 1954. Homogeneous dynamos and terrestrial magnetism, *Phil. Trans. R. Soc. A.,* **247,** 213–278.

Cain, J., Wang, Z., Schmitz, D. & Meyer, J., 1989. The geomagnetic spectrum for 1989 and core-crustal separation, *Geophys. J.,* **97,** 443–447.

Carati, D., Debliquy, O., Knaepen, B., Teaca, B. & Verma, M., 2006. Energy transfers in forced MHD turbulence, *J. Turb.,* **7,** 1–12.

Christensen, U. & Aubert, J., 2006. Scaling properties of convection-driven dynamos in rotating spherical shells and application to planetary magnetic fields, *Geophys. J. Int.,* **166,** 97–114.

Christensen, U. & Olson, P., 2003. Secular variation in numerical geodynamo models with lateral variations of boundary heat flow, *Phys. Earth planet. Inter.,* **138,** 39–54.

Chulliat, A. & Olsen, N., 2010. Observation of magnetic diffusion in the Earth's outer core from Magsat, ørsted and CHAMP data, *J. geophys. Res.,* **115,** doi:10.1029/2009JB006994.

Dormy, E., Valet, J.-P. & Courtillot, V., 2000. Numerical models of the geodynamo and observational constraints. *Geochem. Geophys. Geosyst.,* **1**(10), 1037, doi:10.1029/2000GC000062.

Elsasser, W., 1946. Induction effects in terrestrial magnetism part I. Theory, *Phys. Rev.,* **69,** 106–116.

Finlay, C. & Amit, H., 2011. On flow magnitude and field-flow alignment at Earth's core surface, *Geophys. J. Int.,* **186,** 175–192.

Frisch, U., 1995. *Turbulence: The Legacy of A.N. Kolmogorov*. Cambridge University Press, Cambridge.

Gillet, N., Pais, M. & Jault, D., 2009. Ensemble inversion of time-dependent core flow models, *Geochem. Geophys. Geosyst.,* **10,** Q06004, doi:10.1029/2008GC002290.

Gillet, N., Schaeffer, N. & Jault, D., 2011. Rationale and geophysical evidence for quasi-geostrophic rapid dynamics within the Earth's outer core, *Phys. Earth planet. Inter.,* **187,** 380–390.

Gissinger, C., Dormy, E. & Fauve, S., 2010. Morphology of field reversals in turbulent dynamos, *Europhys. Lett.,* **90,** 49001, doi:10.1209/0295-5075/90/49001.

Glatzmaier, G., Coe, R., Hongre, L. & Roberts, P., 1999. The role of the earth's mantle in controlling the frequency of geomagnetic reversals, *Nature,* **401,** 885–890.

Gubbins, D., 1987. Mechanism for geomagnetic polarity reversals, *Nature,* **326,** 167–169.

Gubbins, D., 2003. Thermal core-mantle interactions: theory and observations, in *Earth's Core: Dynamics, Structure and Rotation*. eds Dehant, V., Creager, K., Karato, S. & Zatman, S., American Geophysical Union, Washington, DC.

Gubbins, D., Barber, C., Gibbons, S. & Love, J., 2000a. Kinematic dynamo action in a sphere: I effects of differential rotation and meridional circulation on solutions with axial dipole symmetry, *Proc. R. Soc. Lond. A,* **456,** 1333–1353.

Gubbins, D., Barber, C., Gibbons, S. & Love, J., 2000b. Kinematic dynamo action in a sphere: II symmetry selection, *Proc. R. Soc. Lond. A,* **456,** 1669–1683.

Gubbins, D., Willis, P. & Sreenivasan, B., 2007. Correlation of Earth's magnetic field with lower mantle thermal and seismic structure, *Phys. Earth planet. Inter.,* **162,** 256–260.

Holme, R., 2007. Large-scale flow in the core, in *Treatise on Geophysics*. Vol. 8, ed. Olson, P., Elsevier Science, London.

Holme, R. & Olsen, N., 2006. Core surface flow modelling from high-resolution secular variation, *Geophys. J. Int.,* **166,** 518–528.

Holme, R., Olsen, N. & Bairstow, F., 2011. Mapping geomagnetic secular variation at the core mantle boundary, *Geophys. J. Int.,* **186,** 521–528.

Jackson, A., 1997. Time-dependency of tangentially geostrophic core surface motions, *Phys. Earth planet. Inter.,* **103,** 293–311.

Jackson, A., Jonkers, A. & Walker, M., 2000. Four centuries of geomagnetic secular variation from historical records, *Phil. Trans. R. Soc. Lond. A,* **358,** 957–990.

Kahle, A., Vestine, E. & Ball, R., 1967. Estimated surface motions at the core surface, *J. geophys. Res.,* **72,** 1095–1108.

King, E., Stellmach, S., Noir, J., Hansen, U. & Aurnou, J., 2009. Boundary layer control of rotating convection systems, *Nature,* **457,** 301–304.

Kolmogorov, A. N., 1941. The local structure of turbulence in incompressible viscous fluid for very large Reynolds numbers, *Proc. USSR Acad. Sci.,* **30,** 299–303.

Kumar, S. & Roberts, P., 1975. A three-dimensional kinematic dynamo, *Proc. R. Soc. Lond. A,* **344,** 235–258.

Kutzner, C. & Christensen, U., 2004. Simulated geomagnetic reversals and preferred virtual geomagnetic pole paths, *Geophys. J. Int.,* **157,** 1105–1118.

Liu, L. & Olson, P., 2009. Geomagnetic dipole moment collapse by convective mixing in the core, *Geophys. Res. Lett.,* **36,** L10305, doi:10.1029/2009GL038130.

Lowes, F., 1974. Spatial power spectrum of the main geomagnetic field, *Geophys. J. R. astr. Soc.,* **36,** 717–730.

McLeod, M., 1996. Spatial and temporal power spectra of the geomagnetic field, *J. geophys. Res.,* **101,** 2745–2764.

Mininni, P., 2007. Inverse cascades and α effect at a low magnetic Prandtl number, *Phys. Rev. E.,* **76,** 026316, doi:10.1103/PhysRevE.76.026316.

Mininni, P., 2011. Scale interactions in magnetohydrodynamic turbulence, *Ann. Rev. Fluid Mech.,* **43,** 377–397.

Moffatt, H., 1978. *Magnetic Field Generation in Electrically Conducting Fluids*. Cambridge University Press, Cambridge.

Olsen, N. & Mandea, M., 2008. Rapidly changing flows in the Earth's core, *Nature Geosci.,* **1,** 390–394.

Olson, P. & Amit, H., 2006. Changes in earth's dipole, *Naturwissenschaften,* **93,** 519–542.

Olson, P. & Christensen, U., 2002. The time averaged magnetic field in numerical dynamos with nonuniform boundary heat flow, *Geophys. J. Int.,* **151,** 809–823.

Olson, P. & Christensen, U., 2006. Dipole moment scaling for convection-driven planetary dynamos, *Earth planet. Sci. Lett.,* **250,** 561–571.

Olson, P., Driscoll, P. & Amit, H., 2009. Dipole collapse and reversal precursors in a numerical dynamo, *Phys. Earth planet. Inter.,* **173,** 121–140.

Olson, P., Coe, R., Driscoll, P., Glatzmaier, G. & Roberts, P., 2010. Geodynamo reversal frequency and heterogeneous core-mantle boundary heat flow, *Phys. Earth planet. Inter.,* **180,** 66–79.

Pais, A. & Hulot, G., 2000. Length of day decade variations, torsional oscillations and inner core superrotation: evidence from recovered core surface zonal flows, *Earth planet. Sci. Lett.,* **118,** 291–316.

Pais, M.A. & Jault, D., 2008. Quasi-geostrophic flows responsible for the secular variation of the Earth's magnetic field, *Geophys. J. Int.,* **173,** 421–443, doi:10.1111/j.1365-246X.2008.03741.x.

Pouquet, A., Frisch, U. & Léeorat, J., 1976. Strong MHD helical turbulence and the nonlinear dynamo effect, *J. Fluid Mech.,* **77,** 321–354.

Rau, S., Christensen, U., Jackson, A. & Wicht, J., 2000. Core flow inversion tested with numerical dynamo models, *Geophys. J. Int.,* **141,** 485–497.

Roberts, P. & Scott, S., 1965. On analysis of the secular variation, 1, a hydromagnetic constraint: theory, *J. Geomagn. Geoelectr.,* **17,** 137–151.

Ryan, D. & Sarson, G., 2007. Are geomagnetic field reversals controlled by turbulence within the Earth's core? *Geophys. Res. Lett.,* **34,** L02307, doi:10.1029/2006GL028291.

Schaeffer, N. & Pais, M., 2011. On symmetry and anisotropy of Earth-core flows, *Geophys. Res. Lett.,* **38,** L10309, doi:10.1029/2011GL046888.

Takahashi, F., Matsushima, M. & Honkura, Y., 2007. A numerical study on magnetic polarity transition in an MHD dynamo model, *Earth Planets Space,* **59,** 665–673.

Voorhies, C., 2004. Narrow-scale flow and a weak field by the top of Earth's core: evidence from Orsted, Magsat, and secular variation, *J. geophys. Res.,* **109,** doi:10.1029/2003JB002833.

Whaler, K., 1986. Geomagnetic evidence for fluid upwelling at the core-mantle boundary, *Geophys. J. R. astr. Soc.,* **86,** 563–588.

Whaler, K. & Davis, R., 1997. Probing the Earth's core with geomagnetism, in *Earth's Deep Interior,* ed. Crossley, D., Gordon and Breach, Amsterdam.

Wicht, J. & Olson, P., 2004. A detailed study of the polarity reversal mechanism in a numerical dynamo model, *Geochem. Geophys. Geosyst.,* **5,** doi:10.1029/2003GC000602.

Yousef, T., Rincon, F. & Schekochihin, A., 2007. Exact scaling laws and the local structure of isotropic magnetohydrodynamic turbulence, *J. Fluid Mech.,* **575,** 111–120.